Journal of Materials Chemistry C

COMMUNICATION

View Article Online
View Journal | View Issue

Cite this: J. Mater. Chem. C, 2014, 2, 6471

Received 31st March 2014
Accepted 16th June 2014

DOI: 10.1039/c4tc00654b

www.rsc.org/MaterialsC

Anomalous compression of a weakly CH···O bonded nonlinear optical molecular crystal†

Weizhao Cai,[a] Jiangang He,[b] Wei Li*[c] and Andrzej Katrusiak*[a]

The organic nonlinear optical crystal, 3-methyl-4-nitropyridine *N*-oxide (POM), exhibits a negative-linear-compressibility (NLC) region as well as exceptionally large positive thermal expansion. High-pressure single crystal X-ray diffraction measurements have revealed an anomalous reversal of NLC at 0.12 GPa, induced by the collapse of the CH···O bonded supramolecular framework and subtle rotations of the nitro group. The initial compression of the weak supramolecular network in the molecular POM crystal is analogous to the hydrostatic responses of the framework crystals with much stronger cohesion forces. Density functional theory (DFT) calculations show that both the subtle conformational distortions and the crystal compression modify the second-harmonic generation (SHG) efficiency of POM.

Weak hydrogen bonds CH···O significantly contribute to the cohesion forces between small organic molecules and biological systems.[1] Previous investigations revealed that pressure not only promotes CH···O interactions in molecular crystals but also modifies the molecular conformation.[2] The conformational conversions of molecules in crystals can be associated with the specific functional features, such as anomalous negative linear compressibility (NLC).[3] Materials with NLC are sought for various technological applications in precise equipment, opto-mechanical and other ultrasensitive devices.[4] Only very few simple inorganic materials demonstrate weak NLC effects.[5] Recently, the NLC was reported in a series of cyanide-bridged coordination polymers,[6] metal–organic frameworks (MOFs)[7] and metal complexes.[8] In these systems, the NLC mechanism can be attributed to the 'wine-rack' or 'lattice-fence' structural motifs.[4a] Apart from this handful of inorganic and hybrid NLC materials, a few NLC organic materials were also discovered. Recently, the anisotropic OH···O hydrogen-bonded 'lattice-fence' network in methanol monohydrate with the NLC of −3.8 TPa^{-1} was reported.[9] Also the wine-rack architecture of weak NH···N and Cl···Cl interactions in 2-(3′-chlorophenyl)imidazoline gives rise to its NLC in the low-pressure range.[10] Here we show that weak CH···O intermolecular interactions can form supramolecular architectures in molecular crystals resulting in anisotropic compression analogous to that of the materials with strong frameworks.[6,7]

Moreover, the nonlinear optical (NLO) properties of organic crystals can be substantially influenced by pressure, which is closely related to structural deformations.[11] In 4-amino-benzophenone, the conformation of the donor and acceptor groups in the molecular structure can modulate the SHG response dramatically.[12] High pressure is an ideal means for changing intermolecular interactions, and therefore it is appropriate for examining the structure–property relationship of nonlinear organic crystals. Herein, we present a systematic high-pressure study of 3-methyl-4-nitropyridine *N*-oxide (POM) crystal (Scheme 1), a commercial NLO material for pico- and femto-second optics in the near-IR range.[13] POM was extensively investigated by X-ray and neutron diffraction.[14] Three phase transitions at 0.8, 2.0 and 6.0 GPa between crystalline phases of POM and an amorphous phase under non-hydrostatic conditions were deduced from Raman spectra.[15] We have probed the pressure-modulated functionalities of this organic material. Our results show that the linear compressibility of the *b*-axis

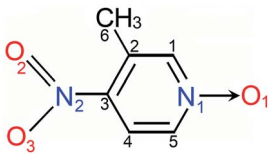

Scheme 1 The molecular structure of POM and its atomic labels.

[a]Faculty of Chemistry, Adam Mickiewicz University, Umultowska 89b, Poznań 61-614, Poland. E-mail: katran@amu.edu.pl

[b]School of Applied and Engineering Physics, Cornell University, Ithaca, New York 14853, USA

[c]Department of Materials Science and Metallurgy, University of Cambridge, Cambridge CB3 0FS, UK. E-mail: wl276@cam.ac.uk

† Electronic supplementary information (ESI) available: Experimental details, Fig. S1–S15, Tables S1–S9 and CIF files. CCDC 979868–979878 and 979897–979912. For ESI and crystallographic data in CIF or other electronic format see DOI: 10.1039/c4tc00654b

switches from negative to positive at 0.12 GPa through an isostructural phase transition induced by the rotations of the nitro group in the POM molecule and the collapse of the CH···O bonded supramolecular framework. DFT calculations reveal the strong effect of the crystal compression and pressure-dependent SHG efficiency.

POM crystallizes in noncentrosymmetric space group $P2_12_12_1$, with one molecule in the asymmetric unit.[14] As shown in Fig. 1, adjacent POM molecules are connected into infinite chains *via* C5H3···O2^b (symmetry code b: x, $y-1$, $1+z$) and C6H6···O1^c (symmetry code c: x, $1+y$, $z-1$) hydrogen-bonds along diagonal directions [011] and [0$\bar{1}$1], respectively. The H-bonded chains are further linked in the [100] direction into a 3-D network through C1H1···O1^a (symmetry code a: $1/2-x$, $-y$, $z-1/2$) and C4H2···O3^d (symmetry code d: $-x$, $y-1/2$, $3/2-z$) bonds. These H-bonds resemble a hinged supramolecular construction of C5H3···O2^b/C6H6···O1^c bonded struts capable of rotating about the C1H1···O1^a/C4H2···O3^d hinges (Fig. 1 and S3†).

Nanoindentation measurements were performed using a three-sided pyramidal Berkovich tip (radius ~ 100 nm) in the continuous stiffness measurement (CSM) mode. The indenter axis was aligned normal to the POM crystal facets {100}, {010} and {001}. The representative load–penetration (P–h) curves obtained on all three facets are shown in Fig. 2, and the average values of the elastic moduli (E) normal to {100}, {010} and {001} are 11.4(2), 15.1(3) and 13.1(2) GPa, respectively, calculated over indentation depths of 200–1000 nm.[16] The significant elastic anisotropy reflects a strong correlation between the mechanical properties and the underlying CH···O bonded strut-hinge supramolecular framework (Fig. 1 and S3†). The [100] direction shows the lowest elastic modulus, because the inter-strut hydrogen bonds are twice less frequent (one H-bond between a pair of molecules) than the H-bonds along the strut (two H-bonds between a pair) orientation. As seen in Fig. 4, the indentation stress along the [010] direction (toward the acute angle $180° - \theta = 80.1°$) can be more absorbed by the rigid hydrogen struts along [011] and [0$\bar{1}$1], compared to that down the [001] direction (toward the obtuse hinge angle $\theta = 99.9°$), which results in higher rigidity along the [010] direction. The anisotropic nanoindentation response is consistent with the crystal hydrostatic compression, much larger along axis a, than those along axes b and c (see below). Notably, significant discontinuities (pop-ins) can be clearly observed from the loading segment of {010} (Fig. 2). The first displacement burst occurred at ~1.26 mN, which refers to the contact pressure of ~0.42 GPa (Fig. S4†). The depths of indentations are of about 20–60 nm, in multiple intervals of the b axis lengths. Such pop-ins have been observed in other organic molecular crystals such as saccharin[17] and aspirin (polymorph I).[18]

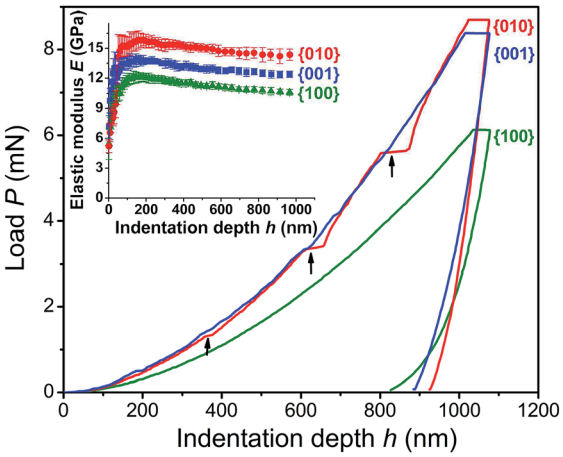

Fig. 2 Representative load–penetration (P–h) curves for POM crystals with {100}, {010} and {001} orientated facets measured using a Berkovich tip. Inset: elastic moduli of POM as a function of indentation depth, wherein each error bar represents the standard deviation from 15 indents. Pop-ins are indicated as arrows.

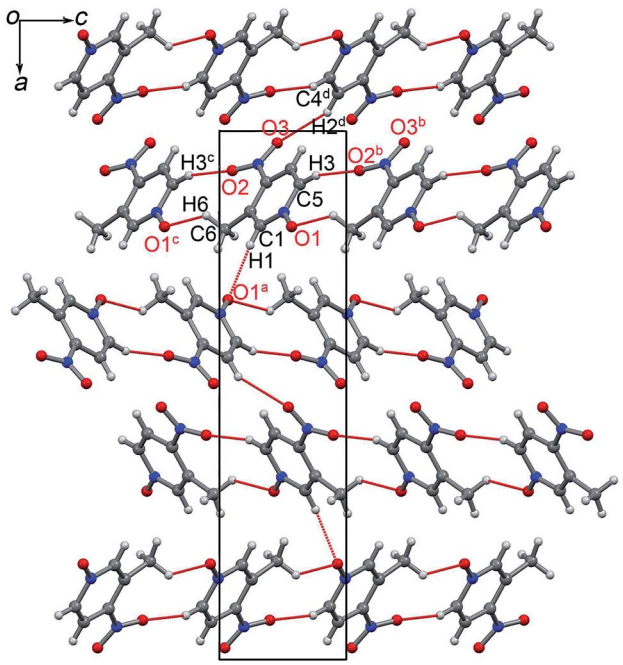

Fig. 1 Crystal structure of POM viewed along the crystal direction [010]. Atom-color code: gray C; red O; blue N; light grey H. The CH···O contacts are shown as red dashes. For clarity, the parallel chains along diagonal directions in other layers were omitted. The symmetry codes are: (a) $1/2-x$, $-y$, $z-1/2$; (b) x, $y-1$, $z+1$; (c) x, $y+1$, $z-1$; and (d) $-x$, $y-1/2$, $3/2-z$.

The relative displacement of the POM molecules along different directions depends on the strength of intermolecular interactions, which could suggest some structural basis for the deformation process involved.[19] The variable-temperature single-crystal X-ray diffraction measurements reveal that the POM crystal exhibits large anisotropic thermal expansion with axis a expanding by 2.2%, and axes b and c expanding about seven times less between 120 and 300 K (Table 1, Fig. S5 and S6†). The pronounced hindrance to the relative molecular motion along the b and c axes corresponds to their much stronger intermolecular interactions compared with that along the a axis, which is consistent with the aforementioned nanoindentation and the below high-pressure X-ray diffraction

Table 1 Linear thermal expansion α (120–300 K) and compressibility coefficients of POM (β_I for 0–0.12 GPa and β_{II} for 0.12–3.57 GPa)

Direction	α (MK^{-1})	β_I (TPa^{-1})	β_{II} (TPa^{-1})
Axis *a*	126.5(18)	37(3)	25.8(2)
Axis *b*	15.8(17)	−33(2)	13.2(9)
Axis *c*	18.0(5)	29.2(5)	14.3(11)

studies. The volume thermal expansion coefficient, α_V of 162(4) MK^{-1}, expected for a molecular crystal, is about five times larger than that of most conventional engineering materials (*e.g.* steel, 35 MK^{-1}).[20] The large PTE magnitude of 126.5(18) MK^{-1} along axis *a* is comparable to that of the well-known framework Prussian blue compounds,[21] and is about four times smaller than that of the record-breaking molecular material (*S*,*S*)-octa-3,5-diyn-2,7-diol.[22]

High-pressure single-crystal X-ray diffraction measurements were carried out with a modified Merrill–Bassett diamond-anvil cell (DAC).[23] One sample crystal was mounted in the DAC, then filled with glycerol (its hydrostatic limit up to 4.0 GPa)[24] as the hydrostatic transmitting medium, and hydrostatically compressed to 0.81 GPa (Fig. S1†); another crystal was isobarically grown in methanol (it remains hydrostatic up to 3.6 GPa)[25] at 1.29 GPa, and compressed up to 3.57 GPa (Fig. S2†). Most strikingly, initially the *b* axis expands up to 0.12 GPa (NLC), above which it reverses to a positive linear compressibility (PLC) (Fig. 3a). Below 0.12 GPa, the NLC coefficient, β_b(I), is −33(2) TPa^{-1}, one fourth of the value (−112 TPa^{-1}) extracted from the indirect Brillouin scattering.[2,26] The NLC-coefficient of POM is larger than those of most reported organic crystals and comparable to that of 1,3-cyclohexanedione (−29(2) TPa^{-1} between 0.11 and 0.52 GPa),[27] and in the same range as the most extreme NLC framework materials, *e.g.* in $Ag_3[Co(CN)_6]$ it is −76(9) TPa^{-1} from 0.1 MPa to 0.19 GPa (ref. 6*a*) and in $Zn[Au(CN)_2]_2$ it is −42(5) TPa^{-1} between 0.1 MPa and 1.8 GPa (ref. 6*b*) (Table S3†). Above 0.12 GPa, the POM crystal compression along the *b* axis becomes positive (Fig. 3a and Table 1). The *a* and *b* axes exhibit the largest and smallest compression (~8.8% for axis *a* and ~3.7% for axis *b*) up to 3.57 GPa, which is consistent with the uniaxial nanoidentification measurements.

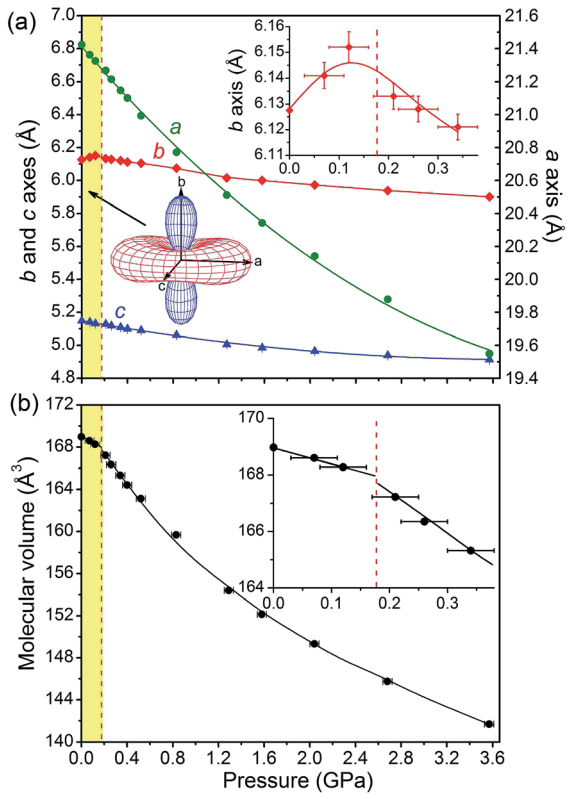

Fig. 3 (a) Crystal lattice parameters of POM as a function of pressure. The inset enhances the negative-to-positive transformation region of the *b* axis compression. The compressibility indicatrix for phase I, with its positive (red) and negative (blue) regions indicated, is shown in another inset. (b) The molecular volume V_m (V/Z) as a function of pressure. The inset shows the linear (phase I) and third-order Birch–Murnaghan (phase II) equation-of-state (EOS) fits to the V_m data. In the main plots error bars are smaller than the symbols used.

There is a clear anomaly in the molecular-volume compression above 0.12 GPa and the crystal becomes considerably softer (Fig. 3b). This $V_m(P)$ anomaly is mainly due to the reversed compression along axis *b*. It is plausible that this anomaly marks an isostructural transition between phase I below 0.12 GPa and phase II above 0.12 GPa. The zero-pressure bulk modulus B_0 of phase I is 23(5) GPa obtained from a linear fit to the diffraction data. In phase II (the PLC region), the third-order Birch–Murnaghan equation of state (EOS) fitted to the $V(P)$ points gives a bulk modulus B_0 of 6.3(10) GPa and a B' of 12.8(22), where B' is the pressure derivative of isothermal bulk modulus.[28] The B_0 magnitudes illustrate the strong increase in compression between NLC and PLC regions. Such pressure-induced softening behaviour is extremely rare and to the best of our knowledge was observed in very few materials, *e.g.* metalloporphyrin.[29]

The unusual NLC response and anisotropic PTE of POM can be attributed to the hinged-network structure and its scissor-like motion (Fig. 1 and 4). The lattice-framework relationships in POM can be expressed as formulae:

$$b = 2r \sin(\theta/2) \quad (1)$$

$$c = 2r \cos(\theta/2) \quad (2)$$

where r is half of the unit-cell bc diagonal (equal to half of the translation along the $[0\bar{1}1]$ direction, see Fig. 4 and S3†), θ is the hinge angle equal to 2arctan(b/c). In the NLC region the hinge angle θ abruptly increases from 99.922(4)° at 0.1 MPa to 100.35(2)° at 0.12 GPa, and the parameter r expands simultaneously, resulting in the expansion of unit-cell dimension *b* and the contraction of perpendicular *c* (Fig. 4). Above 0.12 GPa, after hinge angle θ reaches its maximum opening, it drops back to 100.20(2)° marking the transition to the PLC region. Then angle θ gradually rises to another broad maximum around 1.60 GPa, monotonically decreases to 100.44(2)° at 3.57 GPa. Between 0.21 and 3.57 GPa parameter r is compressed by 0.158(2) Å. As shown in Fig. S7,† the effect of r compression surpasses that of changes

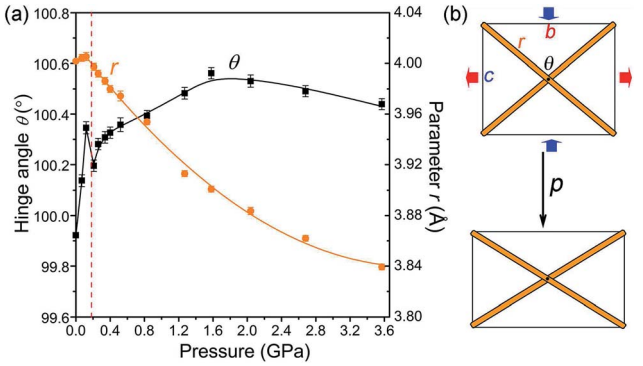

Fig. 4 (a) Hinge angle θ (black squares) and strut length r (orange circles) as a function of pressure. Some error bars are smaller than the symbols used. (b) The schematic illustration exaggerating the compression of diagonal chains in response to the hydrostatic pressure.

in angle θ, the b parameter resumes the PLC according to eqn (1). However, the temperature effect is more subtle, *e.g.* the $r(T)$ elongation exactly correlates with the large PTE, while $\theta(T)$ initially increases with temperature and stops at about 240 K, above which it slightly decreases (Fig. S8†).

In the POM molecule, the nitro group (–NO_2) can rotate about the N2–C3 bond. The nitro oxygen atoms are H-acceptors both in the CH···O bonds along the chain and in the H-bond hinges. Thus the conformation of the nitro group adjusts to strains in the crystal environment. The initial compression of the crystal up to 0.12 GPa increases the torsion angle τ of the nitro group relative to the pyridine ring from 15.7(1)° to 19.4(8)°; at 0.21 GPa it abruptly drops to 16.3(7)° and continues to decrease to 12.1(5)° at 3.57 GPa (Fig. 5 and Table S4†). According to the potential energy calculations, the isolated POM molecule is preferentially stable for τ = 4.6°. The POM conformer at 0.12 GPa is by about 0.17 kJ mol^{-1} higher in potential energy than that at 0.1 MPa (Table S4†). It is characteristic that above the transition to phase II the τ-dependence on pressure is reversed (Fig. 5) and the potential energy at 3.57 GPa is 0.08 kJ mol^{-1} lower than that at 0.1 MPa (Table S7†). The τ angle increases from 14.75(17)° to 15.48(24)° when the temperature increases from 120 to 300 K (Fig. 5).

It is remarkable that there are no abrupt changes in the intermolecular distances; however the shortest CH···O contacts exhibit anomalies at the pressure between phase I and II. For example, C5H3···O2^b (symmetry code b: x, $y-1$, $1+z$) and C4H2···O3^d (symmetry code d: $-x$, $y-1/2$, $3/2-z$) contacts expand with increasing pressure to 0.12 GPa and then they become compressed. It is noteworthy that the hinged C1H1···O1^a/C4H2···O3^d contacts are stiffer than contacts C5H3···O2^b/C6H6···O1^c along the diagonal H-bonded chains (Fig. S9 and Table S6†). The intermolecular contacts mapped on the Hirshfeld surface clearly depict the compression of these CH···O bonds. At still higher pressure, the H···H and CH···O contacts become shorter in phase II, which is apparent from larger red spots on the Hirshfeld surface and shorter distances d_e and d_i in 2D fingerprint plots (see Fig. S10 and S11†).[30] In these fingerprints the CH···O contacts appear as two distinct spikes, while a pair of 'wings' corresponds to C···H contacts. Above 1.5 GPa, all CH···O contacts become less prominent, whereas contacts H···H and C···H are intensified (see relative contributions of each type of contact to the Hirshfeld surface in Fig. S12†).

The pressure effects on linear and NLO properties were explored by DFT calculations. The calculated refractive index is anisotropic in the order of $n_{yy} > n_{xx} > n_{zz}$ (see Fig. S13†), consistently with previous experimental measurements.[13b] The calculated SHG efficiency for the high-pressure structures is shown in Fig. 6. The SHG efficiency strongly depends on the pressure, *i.e.* the d_{36} values of the POM crystal at 0.07 and 0.34 GPa are smaller than that at 0.1 MPa due to less orbital overlap induced by the abruptly increased torsion τ, and it is

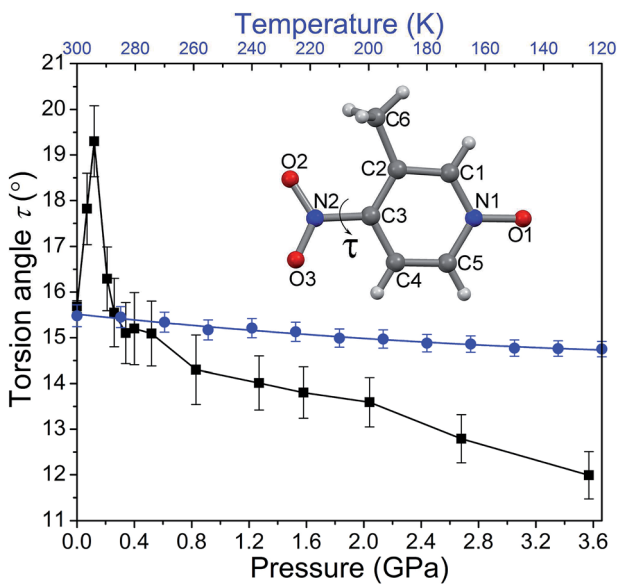

Fig. 5 Torsion angle τ(O2–N2–C3–C4) as a function of temperature (blue circles) and pressure (black squares) in the POM molecule.

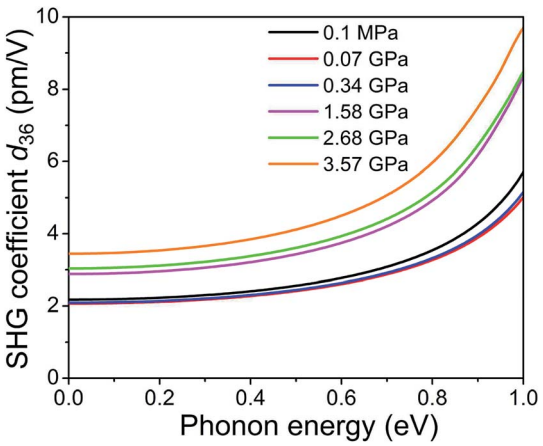

Fig. 6 Frequency-dependent SHG coefficients d_{36} of the POM crystal at the PBE level calculated for high-pressure structures up to 3.57 GPa.

substantially enhanced at higher pressure (*e.g.* the d_{36} magnitude of POM at 3.57 GPa is about 1.7 times higher than that at 0.1 MPa). To establish the NLO effects of torsion τ, we calculated dipole moment μ, and first- and second-order polarizabilities (α and β) of the gas molecules with torsion τ fixed to the experimental value. The calculated magnitudes of μ, α, and β of the gas molecules under ambient conditions well agree with previous calculations.[31] As shown in Fig. S14,† μ, α and β slightly increase with the decreasing torsion τ, due to the larger orbital overlap, so as to the larger charge transfer, in the more planar conformation. Therefore, the compression of the POM crystal plays a more important role in the intensity of SHG efficiency rather than the torsion angle at higher pressure.

Conclusions

In summary, we have shown that the well-known nonlinear organic crystal, POM exhibits the narrow-pressure region of the NLC effect coupled to structural transformations of CH···O bonded architecture and the pressure dependent NLO efficiency. The collapse of this fragile supramolecular construction at 0.12 GPa is reflected in a subtle conformational change and it reverses the NLC. Such a NLC response in a relatively low pressure range can be applied in highly accurate pressure sensors and optic-mechanical transducers. It appears that weakly bonded supramolecular aggregates in molecular crystals can behave similar to framework materials and their properties can drastically change in the relatively low-pressure range.

Acknowledgements

W.C. and A.K. acknowledge the financial support from the Foundation for Polish Science, project TEAM, grant 2009-4/6. W.L. is grateful to the European Research Council for financial support.

Notes and references

1 G. R. Desiraju, *Acc. Chem. Res.*, 1991, **24**, 290.
2 (*a*) K. F. Dziubek, D. Jęczmiński and A. Katrusiak, *J. Phys. Chem. Lett.*, 2010, **1**, 844; (*b*) W. Cai and A. Katrusiak, *J. Phys. Chem. C*, 2013, **117**, 21460.
3 E. V. Boldyreva, T. P. Shakhtshneider, M. A. Vasilchenko, H. Ahsbahs and H. Uchtmann, *Acta Crystallogr., Sect. B: Struct. Sci.*, 2000, **56**, 299.
4 (*a*) R. H. Baughman, S. Stafström, C. Cui and S. O. Dantas, *Science*, 1998, **279**, 1522; (*b*) K. E. Evans and A. Alderson, *Adv. Mater.*, 2000, **12**, 617.
5 (*a*) J. W. E. Mariathasan, L. W. Finger and R. M. Hazen, *Acta Crystallogr., Sect. B: Struct. Sci.*, 1985, **41**, 179; (*b*) D. R. McCann, L. Cartz, R. E. Schmunk and Y. D. Harker, *J. Appl. Phys.*, 1972, **43**, 1432; (*c*) J. Haines, C. Chateau, J. M. Leger, C. Bogicevic, S. Hull, D. D. Klug and J. S. Tse, *Phys. Rev. Lett.*, 2003, **91**, 015503.
6 (*a*) A. L. Goodwin, D. A. Keen and M. G. Tucker, *Proc. Natl. Acad. Sci. U. S. A.*, 2008, **105**, 18708; (*b*) A. B. Cairns, J. Catafesta, C. Levelut, J. Rouquette, A. van der Lee, L. Peters, A. L. Thompson, V. Dmitriev, J. Haines and A. L. Goodwin, *Nat. Mater.*, 2013, **12**, 212; (*c*) A. B. Cairns, A. L. Thompson, M. G. Tucker, J. Haines and A. L. Goodwin, *J. Am. Chem. Soc.*, 2011, **134**, 4454.
7 (*a*) W. Li, M. R. Probert, M. Kosa, T. D. Bennett, A. Thirumurugan, R. P. Burwood, M. Parinello, J. A. K. Howard and A. K. Cheetham, *J. Am. Chem. Soc.*, 2012, **134**, 11940; (*b*) J. M. Ogborn, I. E. Collings, S. A. Moggach, A. L. Thompson and A. L. Goodwin, *Chem. Sci.*, 2012, **3**, 3011.
8 (*a*) H. J. Shepherd, T. Palamarciuc, P. Rosa, P. Guionneau, G. Molnár, J.-F. Létard and A. Bousseksou, *Angew. Chem., Int. Ed.*, 2012, **51**, 3910; (*b*) C. H. Woodall, C. M. Beavers, J. Christensen, L. E. Hatcher, M. Intissar, A. Parlett, S. J. Teat, C. Reber and P. R. Raithby, *Angew. Chem., Int. Ed.*, 2013, **52**, 1.
9 A. D. Fortes, E. Suard and K. S. Knight, *Science*, 2011, **331**, 742.
10 M. Anioła, A. Katrusiak and R. Kia, *CrystEngComm*, 2012, **14**, 6424.
11 (*a*) G. Yang, Y. Li, Z. A. Dreger, J. O. White and H. G. Drickamer, *Chem. Phys. Lett.*, 1997, **280**, 375; (*b*) Y. Li, G. Yang, Z. A. Dreger, J. O. White and H. G. Drickamer, *J. Phys. Chem. B*, 1998, **102**, 5963.
12 E. Marelli, N. Casati, F. Gozzo, P. Macchi, P. Simoncic and A. Sironi, *CrystEngComm*, 2011, **13**, 6845.
13 (*a*) J. Zyss, D. S. Chemla and J. F. Nicoud, *J. Chem. Phys.*, 1981, **74**, 4800; (*b*) M. Sigelle, J. Zyss and R. Hierle, *J. Non-Cryst. Solids*, 1982, **47**, 287.
14 (*a*) M. Shiro, M. Yamakawa and T. Kubota, *Acta Crystallogr., Sect. B: Struct. Crystallogr. Cryst. Chem.*, 1977, **33**, 1549; (*b*) F. Baert, P. Schweiss, G. Heger and M. More, *J. Mol. Struct.*, 1988, **178**, 29.
15 D. Zhang, G. Lan, S. Hu, H. Wang and J. Zheng, *J. Raman Spectrosc.*, 1994, **25**, 327.
16 J. Gong, H. Miao and Z. Peng, *Mater. Lett.*, 2004, **58**, 1349.
17 M. S. R. N. Kiran, S. Varughese, C. M. Reddy, U. Ramamurty and G. R. Desiraju, *Cryst. Growth Des.*, 2010, **10**, 4650.
18 S. Varughese, M. S. R. N. Kiran, K. A. Solanko, A. D. Bond, U. Ramamurty and G. R. Desiraju, *Chem. Sci.*, 2011, **2**, 2236.
19 S. Varughese, M. S. R. N. Kiran, U. Ramamurty and G. R. Desiraju, *Angew. Chem., Int. Ed.*, 2013, **52**, 2701.
20 *Thermal Expansion of Solids*, ed. Y. H. Cho, ASM International, Materials Park, OH, 1998.
21 J. L. Korčok, M. J. Katz and D. B. Leznoff, *J. Am. Chem. Soc.*, 2009, **131**, 4866.
22 D. Das, T. Jacobs and L. J. Barbour, *Nat. Mater.*, 2010, **9**, 36.
23 L. Merrill and W. A. Bassett, *Rev. Sci. Instrum.*, 1974, **45**, 290.
24 L. W. Finger and R. M. Hazen, *J. Appl. Phys.*, 1978, **49**, 5823.
25 D. R. Allan, S. J. Clark, M. J. P. Brugmans, G. J. Ackland and W. L. Vos, *Phys. Rev. B: Condens. Matter Mater. Phys.*, 1998, **58**, 11809.
26 J. Sapriel, R. Hierle, J. Zyss and M. Boissier, *Appl. Phys. Lett.*, 1989, **55**, 2594.
27 A. Katrusiak, *Acta Crystallogr., Sect. B: Struct. Sci.*, 1990, **46**, 246.

28 M. J. Cliffe and A. L. Goodwin, *J. Appl. Crystallogr.*, 2012, **45**, 1321.
29 R. M. Hazen, T. C. Hoering and A. M. Hofmeister, *J. Phys. Chem.*, 1987, **91**, 5042.
30 (*a*) S. K. Wolff, D. J. Grimwood, J. J. McKinnon, M. J. Turner, D. Jayatilaka and M. A. Spackman, *CrystalExplorer. Version 3.0*, University of Western Australia, Crowley, 2012; (*b*) M. A. Spackman and J. J. McKinnon, *CrystEngComm*, 2002, **4**, 378; (*c*) M. A. Spackman and D. Jayatilaka, *CrystEngComm*, 2009, **11**, 19.
31 M. B. Kanoun and B. Champagne, *Int. J. Quantum Chem.*, 2011, **111**, 880.

